



Detecting global irrigated areas by using satellite and reanalysis products

Muhammad Zohaib ^a, Hyunglok Kim ^b, Minha Choi ^{a,*}

^a Environment and Remote Sensing Laboratory, Graduate School of Water Resources, Sungkyunkwan University, Suwon 440-746, Gyeonggi-do, Republic of Korea

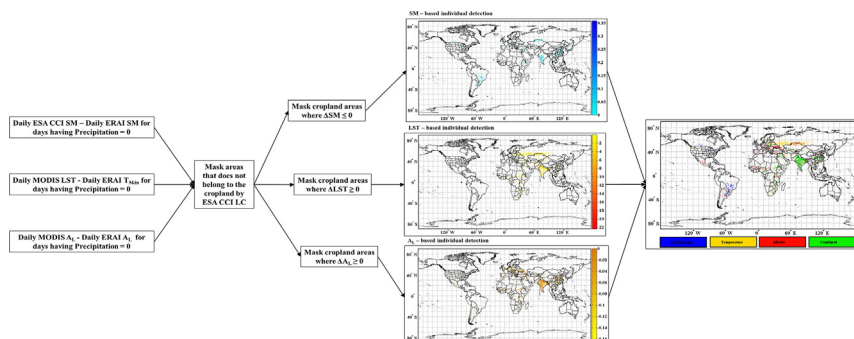
^b The Department of Engineering Systems and Environment, University of Virginia, Charlottesville, VA 22904, USA



HIGHLIGHTS

- Global irrigated areas are identified by combining satellite and reanalysis datasets.
- Soil moisture-based irrigation detection has omitted highly irrigated areas.
- Temperature-based irrigation detection counteracts urbanization.
- Our results demonstrate reasonable accuracy of the proposed irrigation map.

GRAPHICAL ABSTRACT



ARTICLE INFO

Article history:

Received 8 February 2019

Received in revised form 24 April 2019

Accepted 25 April 2019

Available online 26 April 2019

Editor: Ouyang Wei

Keywords:

Soil moisture

Remote sensing

Land surface modeling

Human alteration

Land-atmosphere interaction, Irrigation

Irrigation

ABSTRACT

Despite the importance of irrigation in meeting the world's food demand and as an essential human modification to water and energy cycles, the reliable extent and distribution of the global irrigated areas remain undefined. In this study, an intuitive method is proposed, based on the aftereffects of irrigation, to detect global irrigated areas by combining satellite and reanalysis datasets. The proposed methodology assumes that irrigation is an unmodeled land surface process, while satellite observations can effectively detect irrigation signals in near real-time. The spatial extents of irrigation were derived by calculating the difference between the remotely sensed and reanalysis datasets. To detect the irrigated areas, three irrigation-dependent variables, soil moisture (SM), land surface temperature (LST), and surface albedo (A_L), were used. In the absence of reliable ground truths, the proposed irrigation map was compared to the commonly used global irrigation maps, namely Global Map of Irrigated areas, Global Irrigated Area Map, and recently developed Global Irrigated Areas by Meier et al. (2018). Individual detection by SM, LST, and A_L has discrepancies in detecting irrigation signals in highly irrigated, urbanized, and semi-arid regions. However, by combining the individual detection maps, the proposed method showed reasonable agreement with the reference irrigated maps overlapping with approximately 70% of the irrigated areas. We believe that the proposed method, as stand-alone or in combination with the existing irrigation maps, will benefit the studies regarding water and energy balance closure in near-real time for large-scale land surface models by minimizing the uncertainties in model parameterization.

© 2019 Elsevier B.V. All rights reserved.

1. Introduction

Irrigation supplies artificial water to crops to fulfill global food demand by providing better crop growth conditions and higher average crop yield. It is an essential tool to meet the world's food security,

* Corresponding author at: Department of Water Resources, Graduate School of Water Resources, Sungkyunkwan University, 2066, Seobu-ro, Jangan-gu, Suwon, Gyeonggi-do 440-746, Republic of Korea.

E-mail address: mhchoi@skku.edu (M. Choi).

contributing to 40% of the global agriculture productivities using only 20% of the total cultivable land (Molden, 2007; Schultz et al., 2005). However, irrigation utilizes nearly 70% of global freshwater (Ozdogan et al., 2010) and is a critical human alteration to natural land surface processes (Gordon et al., 2005; Kumar et al., 2015). This alteration modifies the surface energy balance and hydrological cycle by changing the local soil moisture (SM), evapotranspiration (ET), and land surface temperature (LST) (Douglas et al., 2009; Pielke et al., 2011; Ryan et al., 2017; Sacks et al., 2009). The application frequency and quantity of irrigation water have changed in recent years due to climate change effects, advances in irrigation techniques and plant genetic engineering, and rapid population growth (Evans and Sadler, 2008; McDonald and Girvetz, 2013; Riediger et al., 2014; Zhao et al., 2015). Irrigation information is key to several hydrological applications, such as drought- and yield-management and understanding water- and energy-cycles, biosphere-atmosphere interactions, and climate dynamics (Puma and Cook, 2010; Sacks et al., 2009; Wisser et al., 2010; Zhang and Lin, 2016). Recognizing the importance of irrigation as a vital land management practice, studies addressing the effects of irrigation on regional and global climate have rapidly caught the attention of the scientific community (Cheng et al., 2017; Douglas et al., 2009; McDonald and Girvetz, 2013; Pielke et al., 2011; Puma and Cook, 2010).

Despite the importance of irrigation for food security and as an essential human-induced land surface change, accurate information regarding the spatial extent and distribution remains poorly reckoned. Accurate information is required to understand biosphere-atmosphere interactions administered by the planetary boundary layer feedback (Lawston et al., 2015; Qian et al., 2013). This includes modeling energy and water exchanges between land and atmosphere (Boucher et al., 2004; Gordon et al., 2005; Ozdogan and Woodcock, 2006), recognizing irrigation water supply and demand under changing climate (Alcamo et al., 2003; Rosenzweig et al., 2004; Vörösmarty et al., 2000), and managing water resources for global food productivity (Vörösmarty and Sahagian, 2000). Previously, several attempts have been made to estimate the spatial extent of irrigation at regional (Ambika et al., 2016; Ozdogan and Gutman, 2008) and global scales (Loveland et al., 2000; Meier et al., 2018; Salmon et al., 2015; Siebert et al., 2005; Thenkabail et al., 2009). However, none of them represents the actually irrigated areas; rather they depict potential irrigated areas. Moreover, irrigation mapping using these datasets follows a complicated procedure and are difficult to update because of the changing application rate and patterns due to population growth and climate change (Oki and Kanae, 2006). Additionally, previous studies have employed various parameters to detect irrigation, such as ET, vegetation dynamics, and irrigation water requirement, which do not truly reflect the actual application of irrigation water (Meier et al., 2018; Salmon et al., 2015; Thenkabail et al., 2009). Therefore, in this study, specific irrigation-dependent variables were considered to map the spatial extent of global irrigation including SM, LST, and surface albedo (A_L).

Since, irrigation alters local SM, LST, and A_L (Qiu et al., 2016; Shi et al., 2014; Taylor et al., 2012), the concept of backward hydrology (Brocca et al., 2014), in which aftereffects of a phenomenon is used to estimate it, can be used to detect irrigation. Thus, in this study, changes in SM, LST, and A_L were used to estimate the global irrigated areas by combining satellite-based remote sensing and reanalysis datasets. The primary assumption of this study is the absence of irrigation modules in the model datasets (H. Wei et al., 2013; J. Wei et al., 2013), while the spatially continuous satellite observations' ability to detect irrigation signals in near real-time (Kumar et al., 2015; Lawston et al., 2018). A similar concept has been previously employed in various studies at regional scale considering SM only (Kumar et al., 2015; Zaussinger et al., 2019; Zhang et al., 2018). However, SM from the assimilation is considered a model state variable that absorbs errors from other model components (Tuinenburg and Vries, 2017). In ERAI reanalysis, SM is evenly added to or removed from the model when the 2 m air temperature of the model differs from available observations. Tuinenburg and

Vries (2017) found that the additional SM during the assimilation process of ERAI can reasonably represent the irrigation water demand. Hence, in this study, A_L and LST were considered along with SM to estimate the spatial extent of irrigated areas more efficiently.

Land surface model estimates SM, LST, and A_L by using energy and water balance equations. However, the accuracy of model estimates is limited by the type of model used, quality of input data to force model, and understanding of the underlying complex hydrological process (Kim and Lakshmi, 2019; Arnold et al., 2015; Ferguson and Wood, 2011). Moreover, the currently available global land surface models do not include engineering artifacts and neglect some natural systems and processes due to their complex mechanisms (Dee et al., 2011; Kumar et al., 2015; Wood et al., 2011; Zeng et al., 2018). Alternatively, spatiotemporal continuous observations of the earth by satellite remote sensing can potentially capture such unmodeled processes (Hao et al., 2018). Due to this discrepancy of inclusion and omission of anthropogenic effect in satellite and model datasets, respectively, various studies have shown a definite difference in trends between reanalysis SM estimates and satellite SM observations in irrigated areas (Qiu et al., 2016; Zohaib et al., 2017).

Because reliable information on the spatial extents and distribution of actual irrigated areas is limited, the present study proposes a new method to detect global irrigated areas by combining satellite-based remote sensing and reanalysis datasets that can potentially identify the actual irrigated areas of the globe. This study is unique because for the first time a bottom-up approach is utilized to detect the actual global irrigated areas. This global irrigated area map is distinguished from the previous ones in the sense that it marked the actually irrigated areas rather than areas that have potential to be irrigated (Salmon et al., 2015; Siebert et al., 2005; Thenkabail et al., 2009). This was accomplished by comprehending the aftereffects of irrigation, i.e., change in the three hydrological variables such as: SM, LST, and A_L . Following the assumption of this study, the spatial extent of the irrigated areas can be obtained by comparing the time series of these three variables during the irrigation season. Owing to the scarce ground truth data regarding irrigation, the irrigated areas obtained in this study were compared with commonly used irrigation maps, Global Map of Irrigated Areas (GMIA), Global Irrigated Area Map (GIAM), and a recently developed global irrigation map by Meier et al. (2018), now onward termed as M18. This study is a significant step forward in estimating accurate spatial extents of actual irrigated areas of globe, which are considered hotspots in biosphere-atmosphere coupling and will help in minimizing the substantial uncertainties in climate change projections (Lawston et al., 2015; Lawston et al., 2017; Vahmani and Hogue, 2014) and water and energy balance studies (Chen et al., 2018).

2. Materials and methods

The satellite datasets used in this study consist of MODerate-resolution Imaging Spectroradiometer (MODIS) surface products (<https://ladsweb.modaps.eosdis.nasa.gov/>) and European Space Agency (ESA) Climate Change Initiative (CCI) (<https://www.esa-soilmoisture-cci.org/>). The model estimates were obtained from European ReAnalysis-Interim (ERA1) reanalysis products (<https://apps.ecmwf.int/>). MODIS surface products include daily LST and A_L , whereas ESA CCI consists of the combined SM product and land cover product circa 2015. ERA1 products include SM, skin temperature (T_{skin}), and A_L . During preprocessing, all products were resampled to 25 km grid space same as ESA CCI.

2.1. European ReAnalysis-interim datasets

The model variables such as SM, T_{skin} , and A_L that do not incorporate irrigation signals were obtained from ERA1 datasets. Daily SM, T_{skin} (will be stated as LST from model hereafter), and A_L products were obtained with 25 km grid cells. The ERA1 global atmospheric reanalysis dataset

(Dee et al., 2011) was released by the European Center for Medium-range Weather Forecast (ECMWF) in 2011. The assimilation system utilized by ERAI is a 4D variational analysis with 12-hour analysis windows. The reanalysis data were produced by running a fixed version of a numerical weather prediction system, ECMWF's Integrated Forecast System (IFS), 31r2 at a T255 spectral resolution (80 km spatial resolution) with 60 vertical levels. Several atmospheric and surface parameters are freely available at 3-hourly, daily, and monthly datasets covering the period from 1979 to present (Dee et al., 2011). In this study, the topsoil layer (0–7 cm) SM was used. Further details on ERAI products are provided in the supporting information (S1).

2.2. Satellite observations

Observations that contain actual irrigation application information were obtained from two remote sensing datasets; the MODIS and the ESA CCI. MODIS is aboard on two polar orbiting research satellites: the Terra, launched in December 1999 which overpasses at 10:30 and 22:30 local time in descending and ascending orbits, respectively, and the Aqua, launched in May 2002 which overpasses at 1:30 and 13:30 local time in descending and ascending orbits, respectively. MODIS scans the entire globe every 1–2 days working in tandem to obtain a frequent and minimal cloud-contaminated surface view, which provides an opportunity to investigate sub-daily processes. These observations are beneficial in studying the Earth's water cycle, environment, and ocean using 36 spectral bands at three different spatial resolutions; 250 m (channel 1 and 2), 500 m (channel 3 to 7), and 1000 m (channel 8 to 36). In this study, daily LST (MOD11C1) and A_L (MCD43C3) products were obtained from MODIS. Further details on the MODIS products used in this study are provided in the supporting information (S2).

SM observations were obtained from the CCI project, initiated by the ESA in 2012. The ESA CCI SM is a long-term multi-satellite SM data record that is obtained by merging various available active and passive microwave-based SM datasets (Liu et al., 2012). In this study, ESA CCI SM merged product (v04.2) was used, which provides daily products at 25 km spatial resolution at a depth of 0–5 cm. The merged product was produced by combining the active and passive satellite retrievals using an improved weighted-average method (Gruber et al., 2017). The magnitude of the weights was optimized based on the individual random error characteristics of the input data, regarding signal-to-noise ratio, estimated from triple collocation analysis (Gruber et al., 2016; Khan et al., 2018). In addition, it is worth noting that the possibility remains to harness other SM data sources from various active and passive satellite systems, such as the Soil Moisture Active Passive (Entekhabi et al., 2010), the Soil Moisture and Ocean Salinity (Kerr et al., 2001), the Advanced Scatterometer (Wagner et al., 2013), and the Advanced Microwave Scanning Radiometer 2 (Cho et al., 2017) or currently available Global Navigation Satellite System-based SM retrieval systems (Kim and Lakshmi, 2018).

2.3. State-of-the-art global irrigation maps

The major limitation of this study, similar to previous ones (Meier et al., 2018; Ozdogan and Gutman, 2008; Thenkabail et al., 2009), is the unavailability of ground truth observations to verify the performance of the proposed irrigation map. Considering the absence of ground truths regarding the amount and spatial extent of global irrigated areas, we evaluated the performance of the proposed method by comparing with various state-of-the-art irrigation maps at global: GMIA (Siebert et al., 2005), GIAM (Thenkabail et al., 2009), and M18 (Meier et al., 2018) and regional scale: MODIS Irrigated Agriculture Dataset (MIrAD) and irrigated area map of India by Ambika et al., (2016). Before comparison, we resampled these maps to 25 km grid size to make them consistent with the proposed irrigation map.

GMIA is a commonly used irrigation map formulated by the land and water division of Food and Agriculture Organization (FAO) of the United

Nations. This digital global map was developed by compiling the national and sub-national level statistics and geospatial information on the location and extent of area equipped for irrigation in percent units around the year 2005 at five arc minutes spatial resolution (Siebert et al., 2013). Previously, various studies have used this dataset to assess newly developed irrigation maps (Ozdogan and Gutman, 2008; Salmon et al., 2015; Thenkabail et al., 2009) and as a base map for irrigated areas to study irrigation effects on climate across the globe (Pryor et al., 2016; Shi et al., 2014; Tuinenburg and Vries, 2017). This dataset is invaluable information regarding irrigation; however, the statistical information represents the area equipped for irrigation (upper limit) rather than areas that are actually irrigated. Drought, equipment failure, and above average precipitation can all cause the area of irrigated croplands to differ from the area equipped for irrigation (Droogers, 2002; Vörösmarty et al., 2000).

GIAM was developed by the International Water Management Institute (IWMI) based on vegetation cover and potentially irrigated areas at 10 km spatial resolution around year 2000. Vegetation cover was obtained from optical/infrared satellite sensors surface reflectance, whereas potentially irrigated areas were obtained by calculating the evaporative fraction from a simple soil water balance model using in-situ climate observations and FAO digital soil map. The limitation of this map is that optical/infrared remote sensing observations can be severely affected by atmospheric contamination and cloud cover (Thenkabail et al., 2009; Vörösmarty et al., 2000). Moreover, this mapping methodology is mainly based on the evaporative fraction and vegetation index, which do not reflect actual irrigation application.

M18 was recently developed based on GMIA and extending by combining with the high resolution (approximately 1 km) ancillary data comprising (1999–2012) of multi-temporal Normalized vegetation index from SPOT-VGT, agricultural suitability data (Zabel et al., 2014), and WorldClim precipitation (Hijmans et al., 2005). These datasets were combined in a decision tree framework to identify irrigated areas at 1 km spatial resolution as downscaled GMIA and additional areas as active vegetation in the agricultural suitable areas. The results showed that globally, 18% of additional areas were detected in the existing highly irrigated areas including India, the Continental United States (CONUS), and China. M18 had large deviations in Central Asia (Mongolia and Kazakhstan) owing to the classification error in the input data. Further, the discrepancies in the M18 and the existing maps were associated to the definition of irrigation, where GMIA defines irrigated land as an “area equipped for irrigation” and M18 assumes irrigated land where additional water (besides precipitation) is applied to the active vegetation in agricultural suitable areas.

2.4. Ancillary data

The spatial extent of irrigated areas is restricted to cropland by applying cropland mask based on ESA CCI land cover product (<https://www.esa-landcover-cci.org/>) representing the year 2015. Cropland mask was employed because irrigation is mainly applied in cropland to increase agriculture productivity. The overall weighted area accuracy of the ESA CCI land cover product is >71.1% based on the GlobCover 2009 validation dataset (Liu et al., 2018). Moreover, the static masks provided with the ESA CCI SM were also applied to mask out the areas where satellite have problematic observations (Kim et al., 2018; Zhuo and Han, 2017), such as rainforest, vegetation optical depth >0.80 (densely vegetation) and <0.10 (deserts), topographic complexity, and wetland fraction (Ciabatta et al., 2018). In order to separate irrigated and non-irrigated periods, Multi-Source Weighted-Ensemble Precipitation (MSWEP) was used, which is a global precipitation dataset available from 1979 to 2017 at 3-hourly time step and 10 km spatial resolution (Beck et al., 2017; Beck et al., 2018). We resampled it to 25 km to make it consistent with other datasets.

2.5. Methodology

2.5.1. Detecting spatial extent of irrigated areas

In this study, the spatial extents of the irrigated areas were discerned as a positive bias of SM and negative bias of LST and A_L between satellite and reanalysis datasets. Because irrigation causes an increase in local SM, hence conforming to the assumption of this study, the SM of the irrigated pixels for ESA CCI observations would be higher than ERAI SM estimates. Thus, pixels with a positive bias between ESA CCI SM and ERAI SM are assumed as irrigated. Similarly, irrigation causes cooling (Lobell and Bonfils, 2008; Sacks et al., 2009; Shi et al., 2014). Thus, MODIS LST observations will be cooler than the ERAI LST estimates, and a negative bias will represent the irrigated pixels. A_L is defined as the ratio of incident radiation to the reflected radiations, which is altered by an artificial supply of water to soil as irrigation. Since water absorbs solar energy, and irrigation increases soil wetness, thus irrigation causes a decrease in A_L . According to the assumption of this study, MODIS A_L would be lower than the ERAI A_L , and a negative bias will represent an irrigated pixel. To detect irrigated areas based on these three variables, the difference between the satellite observations and model estimates were calculated. The differences in the datasets were masked out on a rainy day based on MSWEP to avoid spontaneous increments in SM by rainfall. Further, if a pixel violated the assumption of this study corresponding to negative bias of SM and positive biases of LST and A_L , were masked out too. The flowchart of the methodology is shown in Fig. 1.

2.5.2. Assessment of the proposed irrigation map

First, the spatial pattern of irrigated areas were detected using three variables (SM, LST, and A_L) individually. Then, the three individual irrigation maps were combined such as the simultaneous detection of irrigated areas by a pair of two variables (SM and LST, SM and A_L , LST and A_L) or by all three variables, concurrently. The three individual and combined detection maps were compared against the GMIA for 2005 at different irrigation fractional coverage, i.e., slightly (5–30%), moderately (30–50%), highly (50–80%), and very highly (>80%); against the GIAM for 2000 as surface water, ground water, and conjunctive use; and

against M18 for 2012. The comparison was done quantitatively for respective years in terms of the number of pixels and percentages of total and overlapped detection (the number of overlapped pixels in certain irrigation class divided by the total number of overlapped pixels of a variable). Secondly, all four irrigation maps (SM, LST, A_L , and combined) were merged to obtained the final irrigation map by the proposed method. The overall detection skill of the proposed method to map the irrigation areas was evaluated by comparing with the three independent and commonly known global irrigation maps; GMIA, GIAM, and M18 and two regional irrigation maps; MIRAD for the CONUS and irrigation area map of India by Ambika et al., (2016) in terms of Producer's (PA) and User's (UA) accuracies, which are defined as:

$$PA = \frac{\text{no.of pixels correctly classified as irrigated in proposed map}}{\text{total no.of irrigated pixels in the proposed map}} \times 100$$

$$UA = \frac{\text{no.of pixels correctly classified as irrigated in proposed map}}{\text{total no.of irrigated pixels in the reference irrigated map}} \times 100$$

PA complements the erroneous detection by the proposed method as omission errors (OE), whereas UA specifies the erroneous detection by the commission errors (CE).

3. Results

3.1. Individual detections

3.1.1. A soil moisture-based irrigation detection map

Fig. 2a shows the spatial distribution of the difference between mean satellite (ESA CCI) and reanalysis (ERAI) SM estimates for 2015. Positive/negative values show that the ESA CCI SM observations are wetter/drier than ERAI SM estimates. Positive values are mainly distributed over India, South America, and southern China. To limit the irrigated areas detection to cropland only, we applied ESA CCI LC cropland mask where both satellite and reanalysis SM showed reasonable accuracy in terms of TC metrics (supporting information S3),

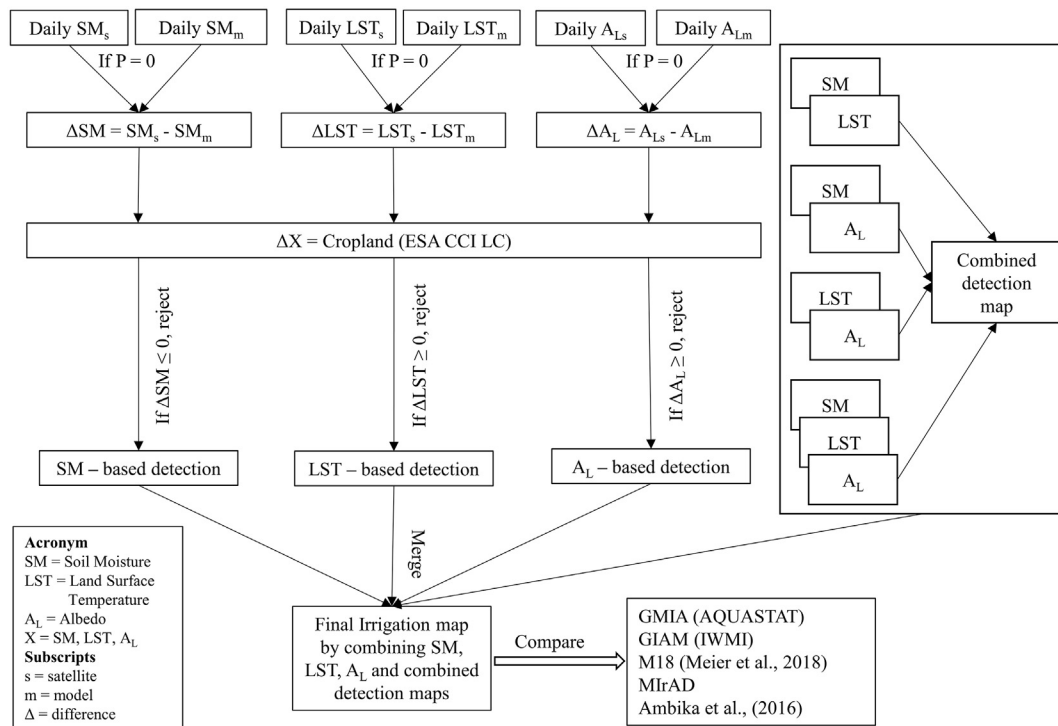


Fig. 1. Flowchart of the methodology for irrigation area detection by soil moisture, temperature, and albedo from satellite and model datasets.

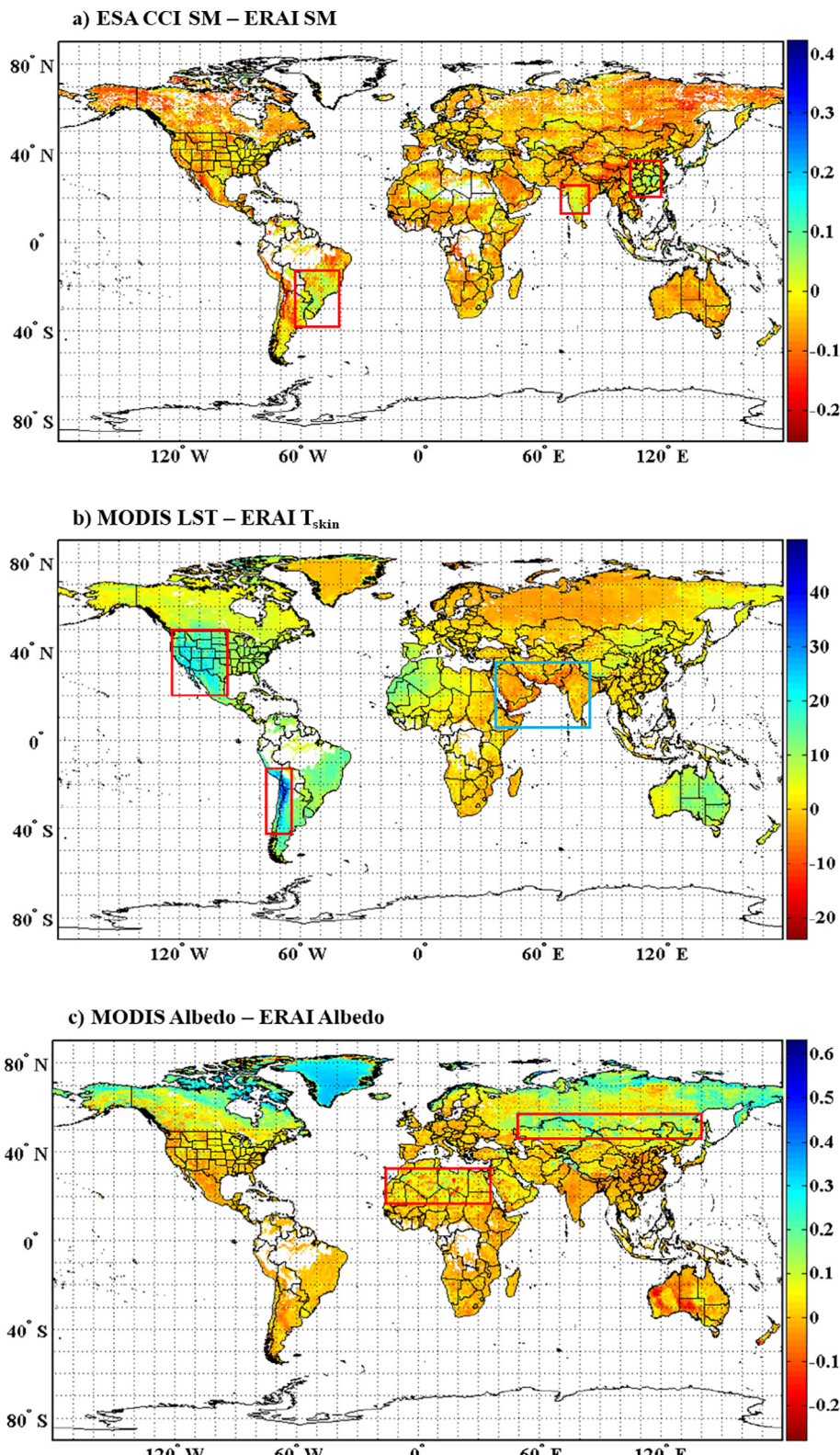


Fig. 2. Spatial distribution of the difference between the satellite and the reanalysis datasets, averaged for daily dataset of 2015 for rain-free period, a) soil moisture, b) temperature, and c) albedo.

mean fMSE <0.5 (Fig. S1). Fig. 3a shows that SM-based irrigation detection map cannot detect very highly irrigated areas, specifically in northern India and California, US, where GMIA shows irrigation >80% (red boxes in Fig. 3b). This result can be explained by an OE resulting from the assimilation process, where the atmospheric model in ERAI is forced

toward the observation. Tuinenburg and Vries (2017) showed that the moisture addition to the ERAI reanalysis process correlates well with blue water use by plants in these areas. The addition of SM thus violates the assumption of this study that the satellite remote sensing SM estimates are higher than the reanalysis SM in irrigated pixels. Overall,

the SM-based irrigation map for 2005 was able to detect 3910 pixels as irrigated compared to the 16,807 pixels in the GMIA map (31%) in which 53.32% pixels overlapped. Quantitatively, the substantial difference between GMIA and the proposed method's irrigation map might be associated with the difference in definitions of irrigation and observational errors. For example, GMIA considered a pixel as irrigated if it has been equipped for the irrigation whereas the proposed method only detects actually irrigated pixels. In terms of pixels identified with different levels of irrigation according to the GMIA, the SM detects 60.43%, 22.59%, 14.67%, and 2.32% in slightly, moderately, highly, and very highly irrigated areas, respectively (Table 1). This result indicates that the SM-based irrigation detection has a limitation in highly irrigated areas caused by the assimilation process of ERAI SM. Moreover, the sensitivity of SM-based irrigation detection increases when application efficiency decreases (Lawston et al., 2015; Zaussinger et al., 2019), thus, SM-based irrigation detection in this method is highly sensitive to gravity irrigation (i.e., flood and furrow) and less sensitive toward sprinkler and drip-irrigation.

3.1.2. A temperature-based irrigation detection map

Fig. 2b shows the difference between mean MODIS LST and mean ERAI LST for 2015. Generally, a highly positive bias can be observed in the western part of both northern and southern America (red boxes in Fig. 2b), and negative bias in India, the middle east, and northeastern Africa (blue box in Fig. 2b). To detect irrigated areas, pixels that violate the assumption of this study (i.e., LST difference ≥ 0) and the pixels that do not belong to cropland were masked out. The LST-based irrigation detection map (Fig. 3b) identified irrigated areas in India, the Indus basin of Pakistan, the southern Volga region in Russia, and the southeastern African continent. The spatial patterns of LST-based irrigated areas in India and Pakistan are identified quite satisfactorily compared to state-of-the-art irrigation maps; however, the irrigated area in China, the Huang-Huai-Hai plain (red box (1) in Fig. 3b), which is one of the world's most highly irrigated area, was missed. Similarly, the highest irrigated area of US, California, is also missing in the LST-based irrigation detection (red box (2) in Fig. 3b). This OE might be caused by regional urbanization, which cancels out the cooling effect of

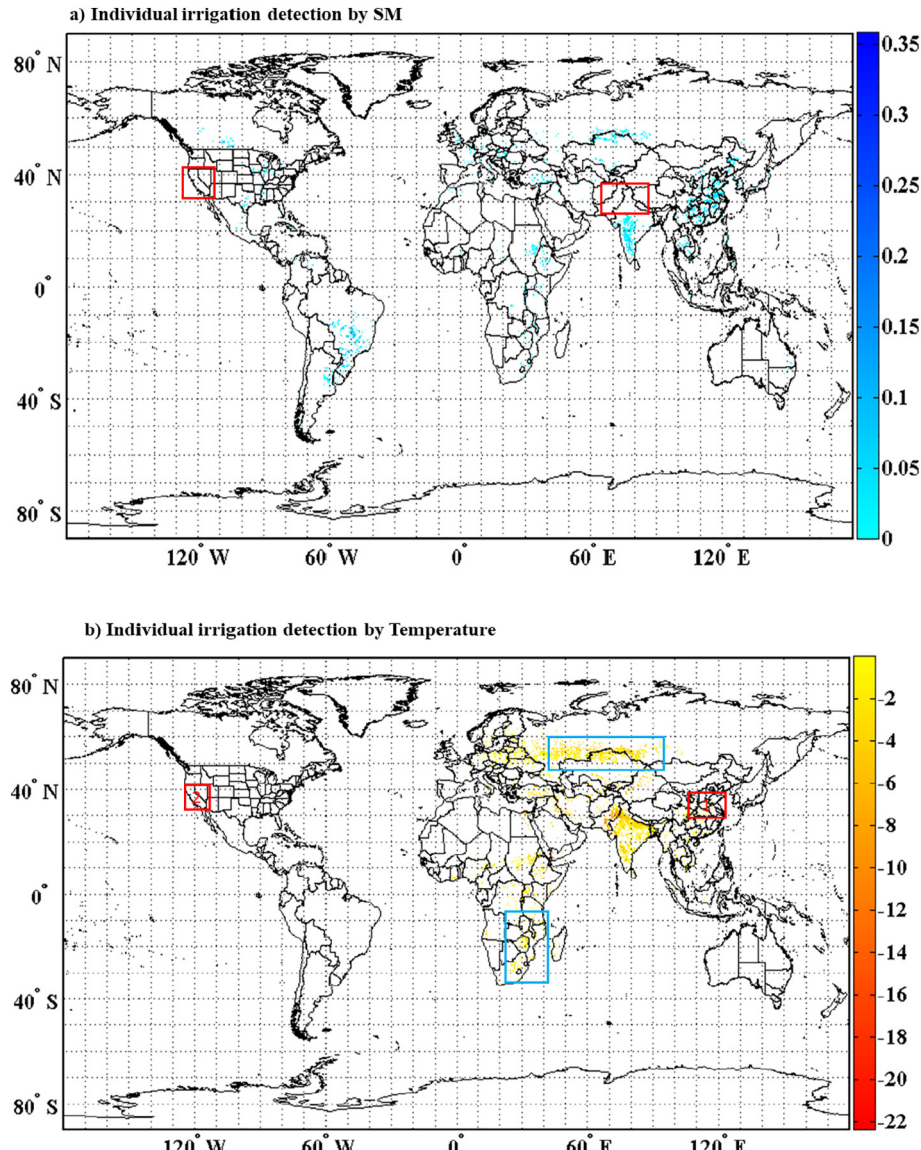


Fig. 3. Spatial distribution of irrigated areas detected by a) soil moisture, b) Temperature, c) Albedo, and d) combined soil moisture, temperature, and Albedo. The spatial extents of irrigated regions were obtained by masking the pixels that violates the assumption, that is, the negative difference of SM and positive difference of LST and albedo. Further, ESA CCI LC cropland masking was applied to restrict the spatial extent of irrigation to the agricultural areas only.

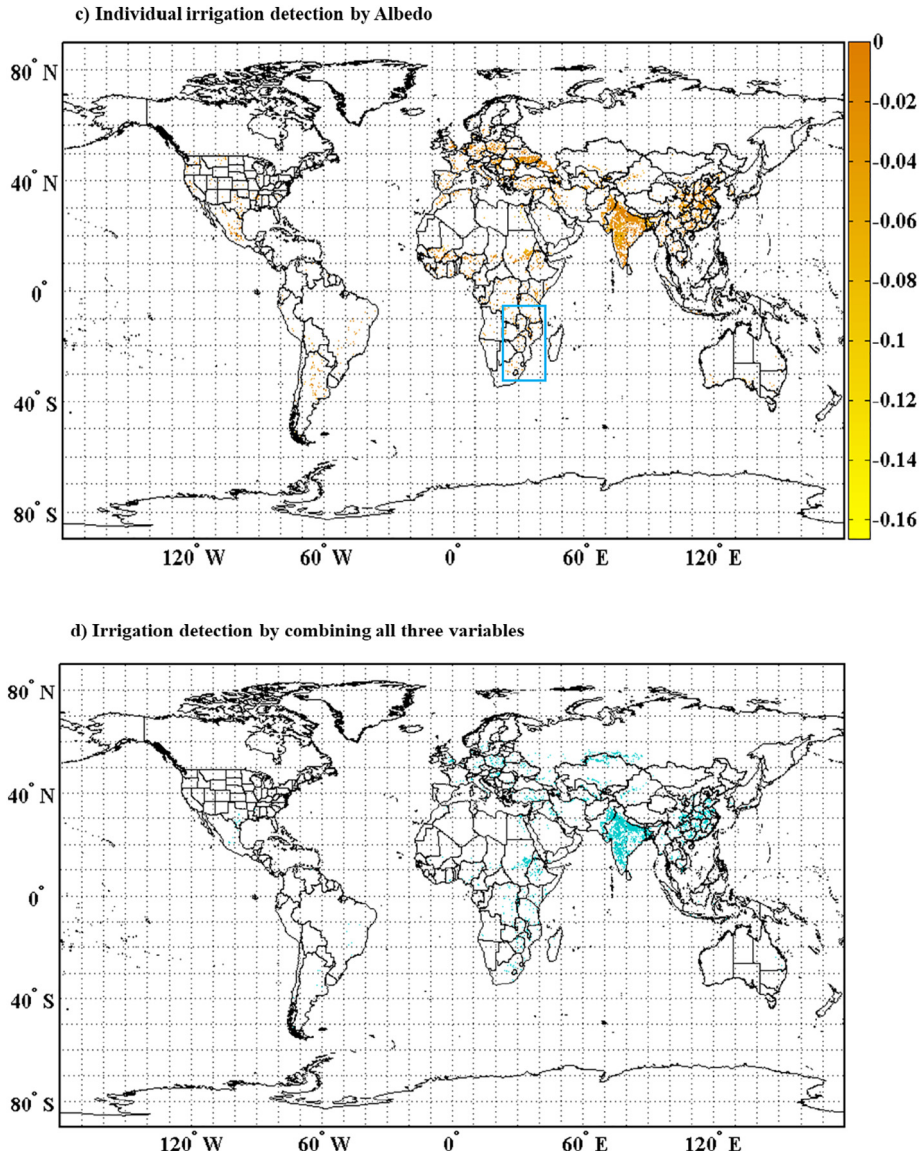


Fig. 3 (continued).

irrigation (Shi et al., 2014). Zhou et al. (2004) confirmed warming of mean LST over southeast China due to urbanization. Similarly, Lobell and Bonfils (2008) showed that the urbanization near irrigated areas reduces the cooling effect caused by irrigation in California. Thus, the warming effect of urbanization and the cooling effect of irrigation in a pixel may cancel out each other, and the irrigated areas might not be marked. Moreover, the LST-based irrigation detection identifies irrigated areas in the semi-arid climate of southeastern Africa and Volga, Russia (blue boxes in Fig. 3b). However, these areas were neither represented by the reference maps, as irrigated, nor detected by SM. This CE can be explained by the fact that ERAI LST overestimates MODIS LST in arid and semi-arid climates because surface energy fluxes are misrepresented due to imperfections in the parameterization of aerodynamic resistance and partitioning between latent and sensible heat fluxes (Garand, 2003; Umair et al., 2018; Wang et al., 2014; Zheng et al., 2012). Previously, similar biases were found in the ERAI associated with the limitation in the surface scheme for heat and momentum that used a fixed map of leaf area index and tabulated values of roughness lengths (Trigo et al., 2015; Trigo and Viterbo, 2003). Thus, these limitations falsely fulfilled the assumption of this study and caused erroneous

detection of irrigation in these areas. Quantitatively, the assumption associated with LST-based irrigation detection identifies 7851 pixels as irrigated for 2005, out of which 40.77% overlapped with that of GMIA. In terms of pixels equipped with a different level of irrigation according to the GMIA, LST detects 39.85%, 20.52%, 22.94%, and 16.68% in slightly, moderately, highly, and very highly irrigated areas, respectively (Table 1). Specifically, LST-based irrigation detection can detect micro-irrigation that barely changes SM and A_L . However, it does influence the local LST due to repartitioning of latent and sensible heat fluxes (Campra et al., 2008).

3.1.3. An albedo-based irrigation detection map

Fig. 2c shows the spatial distribution of the difference between daily means of MODIS A_L and ERAI A_L for 2015. Generally, negative bias in MODIS is prominent across the globe except for the Sahara Desert and the southern boundary of the snow line, i.e., north of 40°N, (marked in the red boxes in Fig. 2c). The positive bias around the southern boundary of the snow might be caused by ERAI, which underestimates the fraction of ground covered by snow for shallow snow depths (Oleson et al., 2003). Moreover, the positive MODIS bias over desert regions

Table 1

Quantitative assessment the proposed irrigation map against GMIA, FAO irrigation map, for slightly (5–30%), moderately (30–50%), highly (50–80%), and very high (> 80%) irrigated areas. The percentage refers to the number of overlapped pixels in certain irrigation class divided by the total number of overlapped pixels.

Proposed Irrigation map of this study/GMIA	Slightly (5–30%)	Moderately (30–50%)	Highly (50–80%)	Very highly (> 80%)	Total		
					Overlapped	New detection	Total
Soil moisture	No. of pixels	1260	471	306	48	2085	1825
	Percentage	60.43	22.59	14.67	2.32	53.32	46.68
Temperature	No. of pixels	1204	620	693	504	3021	4830
	percentage	39.85	20.52	22.94	16.68	40.77	61.52
Albedo	No. of pixels	2326	1043	1019	462	4850	5454
	Percentage	47.96	21.51	21.01	9.53	47.07	53.93
Combined	No. of pixels	1439	725	773	433	3370	2046
	Percentage	42.70	21.51	22.94	12.85	62.22	5416

might be explained by the unique spectral properties of soils that are not accounted in the ERAI (Oleson et al., 2003; Tsvetinskaya et al., 2002). Generally, the A_L -based irrigation detection map identifies both low and high irrigated areas quite well in India, China, Pakistan, and Europe (Fig. 3c). However, like LST-based irrigation detection, A_L -based irrigation detection map also detects irrigated areas in the southwestern part of the African continent including Ethiopia, Tanzania, Mozambique, and Zimbabwe (blue box in Fig. 3c), erroneously. This CE can similarly be explained by the misrepresentation of the surface energy fluxes in the ERAI (Trigo et al., 2015). Moreover, Tuinenburg and Vries (2017) showed that in these areas SM addition by assimilation positively correlates with the precipitation bias rather than blue water demand, which corroborates false detection of irrigation by LST and A_L . Moreover, A_L -based irrigation detection compensates for the SM-based irrigation detection in the highly irrigated areas and LST-based irrigation detection in the urbanized areas, where irrigation cooling is counteracted by the regional urbanization. For 2005, A_L detects 10,304 pixels as irrigated, which is almost triple of SM-detection alone, out of which 47.07% area overlapped with that of the GMIA. The percentage of detections were higher in the slightly (47.96%) followed by moderately (21.51%), highly (21.01%), and very highly (9.53%) irrigated areas, respectively (Table 1).

3.1.4. A combined irrigation detection map

Fig. 3d shows the spatial distribution of global irrigated areas detected by combined irrigation detection map. The combined detection was defined as the simultaneous detection of irrigated areas by a pair of two variables (SM and LST, SM and A_L , or LST and A_L) or by all three variables, concurrently. Spatially, the patterns of irrigated areas by combined detection are mostly distributed over India, China, Pakistan, Europe, and southeastern Africa. Compared to the existing global irrigation maps, irrigated areas of Asia and Europe were well outlined. However, as discussed earlier the irrigated areas in Africa were erroneously detected by LST and A_L because of uncertainty in ERAI to represent the surface energy fluxes in arid and semi-arid regions. Quantitatively, the combined detection map for 2005 was comparative to that of SM detection individually, and the total number of pixels detected was 5416. Moreover, detection in the very highly irrigated areas (>80%) improved from around 2.32% (by SM individually) to 12.85% (combined), where SM is limited in detecting the irrigated areas as a model state variable. Similarly, in areas with slightly, moderately, and highly irrigated areas, the overlapped detection was 42.07%, 21.51%, and 22.94%, respectively (Table 1).

3.2. Comparison with state-of-the-art global irrigation maps

The final proposed irrigation map was obtained by integrating all individual detection maps, and the overall detection was compared with the three state-of-the-art global irrigated maps. The spatial patterns of irrigated areas based on the proposed method matched well with the reference irrigation maps except in the arid and semi-arid cropland

regions of southeastern Africa and Volga, Russia (blue box in Fig. 4a). Compared to the GMIA (Fig. 4b), highly irrigated areas of China, India, and Pakistan were detected well in the combined detection (green color in Fig. 4a), whereas the moderately irrigated areas of Europe are mainly detected by A_L alone (red color in Fig. 4a). The surface water irrigated areas from GIAM (blue color in Fig. 4c) was mostly detected by a combined detection or A_L -based detection alone. However, the conjunctive ground and surface water irrigation in northeast China and the CONUS were detected by SM alone. Finally, a comparison with the most recent global irrigated area maps by Meier et al. (2018) (Fig. 4d) showed that overall spatial patterns of irrigated areas in both maps matched satisfactorily in Asia, Europe, and the CONUS. The PA was approximately 70% with the three benchmarked global irrigation maps. Specifically, the PA for the proposed irrigation map for 2005 (Fig. S2b) against the GMIA was 69.06% (Table 2), out of which the highest percentage was for the very highly irrigated areas, 86.71%, followed by highly irrigated areas, 78.07%, moderately irrigated areas, 73.53%, and slightly irrigated areas, 62.47%. The PA for the proposed irrigation map for 2000 (Fig. S2a) against GIAM irrigation maps was 60.27%, where detection of the three attributes, i.e., surface water, groundwater, and conjunctive water used for irrigation were 56.96%, 74.54%, and 79.76%, respectively. While compared to M18 for 2012, the PA for the proposed irrigation map for 2012 (Fig. S2c) was 73.37%. With all the three benchmarked irrigation maps, the proposed irrigation map showed low UA, specifically, 36.81%, 44.41%, and 21.07% with GMIA, GIAM, and M18, respectively. This specifies high CE associated to the spurious representation of energy fluxes by ERAI in arid and semi-arid regions of Africa and Volga, Russia.

3.3. Comparison with regional/local scale irrigation datasets

The proposed irrigation map was assessed regionally by comparing with MIRAD over the CONUS for 2012 (Ozdogan and Gutman, 2008) and remotely sensed high-resolution irrigation map over India (Ambika et al., 2016) for 2015. The results of regional/local scale assessment are demonstrated in Table 3. Overall, the proposed irrigation map did not match well with the MIRAD irrigation map in the CONUS. The low PA (33.33%) and UA (19.31%) specify substantial OE and CE in the proposed method, respectively. The OE was primarily centered in the arid regions of the western CONUS (Colorado, Idaho, New Mexico, Utah, Wyoming), where irrigation practices are dispersed and heterogeneous, thus, mainly constrained to canyons (Zaussinger et al., 2019). Consequently, coarse-scale irrigation map of this study was unable to identify the small scale irrigation practices of these areas. Conversely, the CE mainly prevails in humid regions of the eastern CONUS (Illinois, Indiana, Iowa, and Ohio), where irrigation is mainly supplemental. Despite these OE and CE, the proposed irrigation map closely agreed to MIRAD in key irrigated areas such as California (PA = 31.04% and UA = 61.36%), Washington (PA = 59.09% and UA = 54.17%), and Mississippi (PA = 80.00% and UA = 61.64%). In India, the proposed irrigation map showed good agreement with the irrigation map by Ambika et al.

(2016). The results in terms of PA and UA (71.97% and 70.44%) specifies low OE and CE. This result corroborates the ability of the proposed method to detect irrigated areas over India. Moreover, a recent study by Singh et al. (2017) also showed that AMSR-E could detect the shifting time of the irrigation practices in north western India. Moreover, the proposed irrigation map was assessed with the field inventory data compiled by the University of Nebraska by using multi-year Landsat and aerial imagery around year 2005. The results showed strong agreement exhibiting high values of PA (78.82%) and UA (81.23%).

To conclude, the existing global irrigation maps are a substantial source of information for the spatial extent of irrigation; however, depending on the data or method used, they certainly have shortcomings in representing the actual global irrigated areas. For example, the FAO maps were primarily based on statistical information for 2005. However, the actual area of irrigated land may increase or decrease driven by each year's water supply and demand (Wisser et al., 2008). Moreover, climate change, advances in genetic engineering and other agriculture-based technologies, and virtual water trade can reshape the spatial distribution of irrigated areas. Similarly, IWMI's GIAM was

developed based on vegetation cover and potential of areas for irrigation. However, these variables do not directly link to actual irrigation. Recently, Meier et al. (2018) revised the global irrigation maps by combining statistics, remote sensing, and agriculture suitability data using multi-decision tree approach and a multi-temporal vegetation index, i.e., Normalized Difference Vegetation Index data. However, their results deviate from official statistics because of classification errors in the input datasets. A major issue with the existing global irrigation maps is the inconsistency associated with the definition of irrigation and reference year. Moreover, these irrigation maps follow a complicated procedure and are difficult to update because of the changing application rate and patterns due to population growth and climate change (Oki and Kanae, 2006). Additionally, previous studies have employed various parameters to detect irrigation, such as ET, vegetation dynamics, and irrigation water requirement, which do not truly reflect the actual application of irrigation water (Meier et al., 2018; Thenkabail et al., 2009). Thus, it is very important to develop irrigation maps considering variables that are directly linked to the irrigation application to represent actual irrigated areas rather than potential irrigated areas. In this regard,

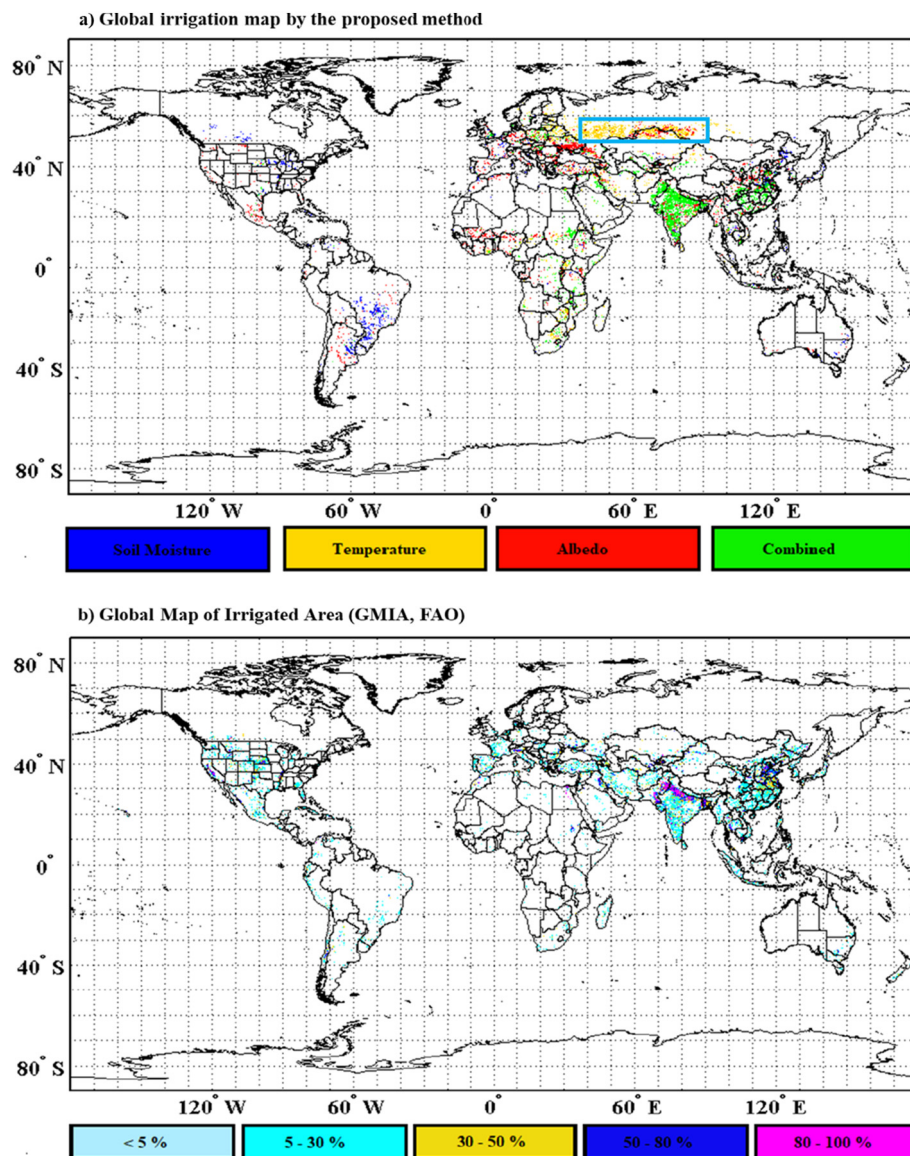


Fig. 4. Spatial extent of global irrigated areas (a) Combined soil moisture, temperature, and albedo in this study and state-of-the-art global irrigation maps (b) Global map of irrigated areas, FAO, (c) Global irrigated area map, IWMI, (d) Global irrigated areas by Meier et al. (2018).

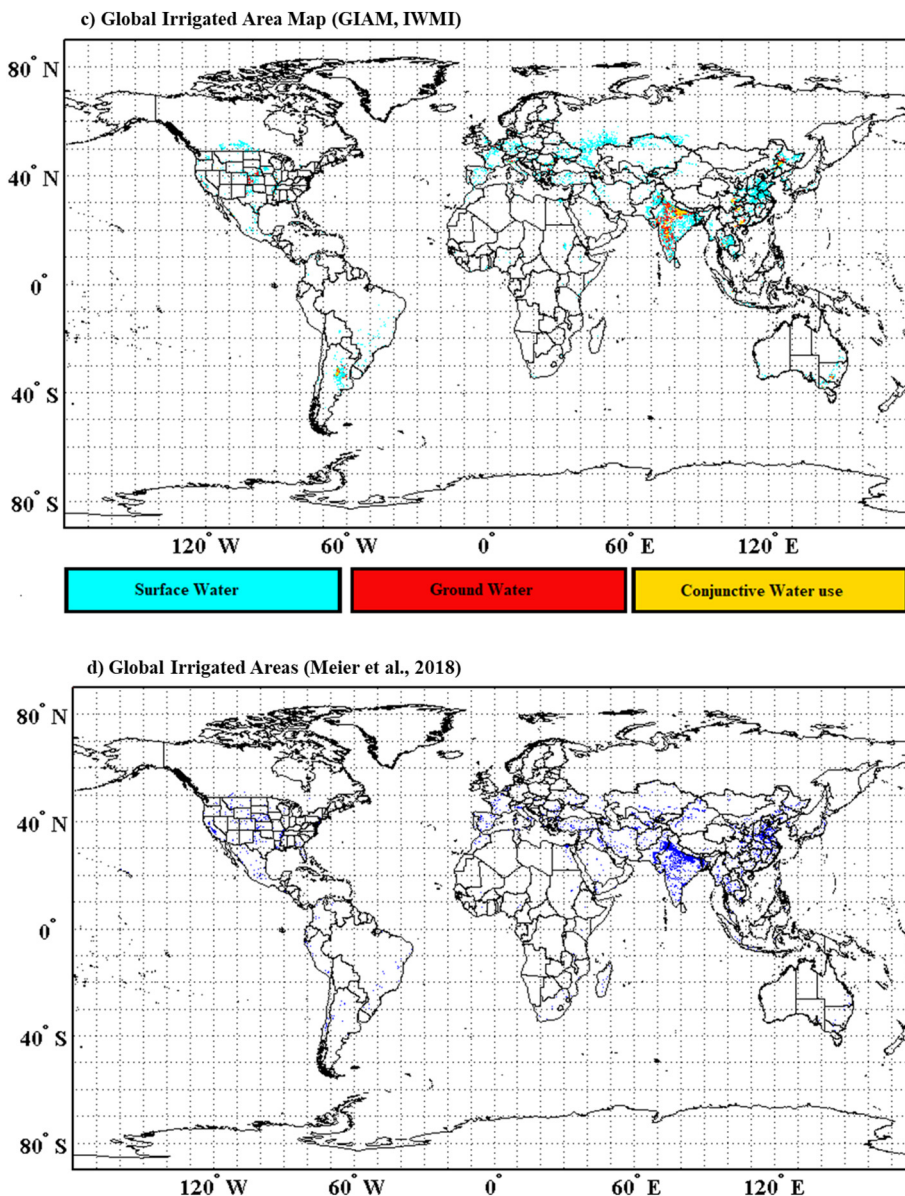


Fig. 4 (continued).

this study utilized the concept of backward hydrology to detect global irrigated areas. The major advantage of the currently proposed method is to obtain irrigation map depicting actual irrigated areas rather than areas that have potential to be irrigated. Secondly, LST- and A_L -based irrigation detection has the potential to detect the micro-irrigation which do not influence the local SM, directly. Thirdly, this method is quite simple, easily replicable, dispensable to training datasets, and capable of mapping historical irrigated areas. Currently, the high temporal resolution of the satellite and modeled datasets have not been manifested directly in this study, however, it can easily be improvised to identify the irrigated areas in near-real time due to spatio-temporal continuous observations from satellite and reanalysis simulations. Moreover, this method can further be utilized to quantify the global irrigation water use, as recently derived by Zaussinger et al. (2019) over the CONUS. Apart from the above-mentioned advantages, we acknowledged the potential limitations of the current method, i.e., the coarse-spatial resolution and violation of the assumption due to systematic errors of the datasets. However, these can be overcome in the future by evolution of satellite remote sensing and improved model parameterization.

Above all, we believe that the method proposed in this study, as stand-alone or in combination with the previously developed map, will add value to accurately detect the spatial extents of irrigated areas that are hotspots for biosphere-atmosphere interactions and minimize the substantial uncertainties in climate change projections.

4. Conclusion

Despite its importance in world food security and impact on local and regional climates, reliable information on the spatial extent of irrigated area remains uncertain. To address this shortcoming, an intuitive method was proposed to detect and verify the spatial extent of global actual irrigated areas using the aftereffects of irrigation, i.e., change in SM, LST, and A_L . This was accomplished by following the assumption that modeled datasets do not incorporate irrigation schemes, whereas satellite-based remote sensing has the potential to capture irrigation signals (Kumar et al., 2015; Lawston et al., 2018). The comparison with the three state-of-the-art irrigation maps, developed by the FAO (GMIA), IWMI (GIAM), and M18 showed that the individual detections

Table 2

Accuracy assessment of the proposed irrigation map against the three state-of-the-art global irrigation maps.

Method	Attributes	Producer's accuracy (%)	User's accuracy (%)
GMIA (FAO)	Overall	69.06	36.81
	Slightly (5–30%)	62.47	–
	Moderately (30–50%)	73.53	–
	Highly (50–80%)	78.07	–
	Very highly (>80%)	86.71	–
	Overall	60.27	44.41
GIAM (IWMI)	Surface water	56.96	–
	Ground water	74.54	–
	Conjunctive use	79.46	–
Meier et al. (2018)		73.37	21.07

by SM, LST, and A_L had discrepancies due to uncertainties in the datasets. For example, SM was unable to detect very highly irrigated areas in India and California, the CONUS (> 80% according to GMIA), and LST and A_L detected false irrigated areas in the semi-arid regions of Volga, Russia, and Southeastern Africa. Generally, the final irrigated area map obtained by merging the individual detection maps (SM, LST, A_L , and combined) matched well with the three state-of-the-art global irrigation maps and regional to local scale irrigation data, exhibiting PA of approximately 70%. The irrigation map based on the proposed method for 2015 is available for download at (http://ersl.skku.edu/bbs/board.php?tbl=notice&mode=VIEW&num=8&category=&findType=&findWord=&sort1=&sort2=&it_id=&shop_flag=&mobile_flag=&page=1), and is available from the authors on request.

Overall, the spatial extents and distributions of actually irrigated areas obtained in this study, as a stand-alone or in combination with the existing irrigation maps, will improve our understanding of biosphere-atmosphere interaction, minimizing uncertainties in the climate projections, and benefits climate researcher to define future scenarios regarding changes in the extent of irrigated areas. Moreover, future research will focus on quantifying irrigation water and irrigation scheduling for better crop production.

Acknowledgment

We are thankful for the availability of the ESA CCI SM and LC data from ESA website, Albedo, T_{skin} and SM form ERA-Interim ECMWF website, MODIS albedo, and LST from LAADS DAAC website, GMIA irrigation map from FAO website, GIAM irrigation map from IWMI website, Early Warning and Environmental Monitoring Program, USGS, for providing MIRAD-US irrigation map, Ambika et al. (2016) for providing irrigation maps of India, and University of Nebraska, CALMIT, for field scale irrigation data for Nebraska.

This research was supported by Space Core Technology Development Program through the National Research Foundation of Korea (NRF) funded by the Ministry of Science and ICT (NRF-2014M1A3A3A02034789).

This work was supported by the National Research Foundation of Korea (NRF) grant funded by the Korea government (MSIT) (NRF-2016R1A2B4008312).

Table 3

Accuracy assessment of the proposed irrigation map at the regional/local scale.

Region	Reference dataset	Producer's accuracy (%)	User's accuracy (%)
Entire CONUS	MIRAD	33.33	19.31
California	MIRAD	31.04	61.36
Mississippi	MIRAD	80.00	61.64
Washington	MIRAD	59.09	54.17
Nebraska	University of Nebraska	78.82	81.23
India	Ambika et al. (2016)	71.97	70.44

Declaration of interest

The authors declare that there is no conflict of interests regarding the publication of this paper.

Appendix A. Supplementary data

Supplementary data to this article can be found online at <https://doi.org/10.1016/j.scitotenv.2019.04.365>.

References

- Alcamo, J., Döll, P., Henrichs, T., Kaspar, F., Lehner, B., RÖSch, T., & Siebert, S. (2003). Global estimates of water withdrawals and availability under current and future "business-as-usual" conditions. *Hydrological Sciences Journal*, 48(3), 339–348. doi: <https://doi.org/10.1623/hysj.48.3.339.45278>
- Ambika, A.K., Wardlow, B., Mishra, V., 2016. Remotely sensed high resolution irrigated area mapping in India for 2000 to 2015. *Scientific Data* 3, 160118. <https://doi.org/10.1038/sdata.2016.118>.
- Arnold, J.G., Youssef, M.A., Yen, H., White, M.J., Sheshukov, A.Y., Sadeghi, A.M., ... Skaggs, R.W., 2015. Hydrological processes and model representation: impact of soft data on calibration. *Trans. ASABE* 58 (6), 1637–1660.
- Beck, H.E., Van Dijk, A.I., Levizzani, V., Schellekens, J., Gonzalez Miralles, D., Martens, B., De Roo, A., 2017. *MSWEP*: 3-hourly 0.25° global gridded precipitation (1979–2015) by merging gauge, satellite, and reanalysis data. *Hydrol. Earth Syst. Sci.* 21 (1), 589–615.
- Beck, H. E., Wood, E. F., Pan, M., Fisher, C. K., Miralles, D. G., van Dijk, A. I., ... Adler, R. F. (2018). MSWEP V2 global 3-hourly 0.1° precipitation: methodology and quantitative assessment. *Bulletin of the American Meteorological Society* (2018).
- Boucher, O., Myhre, G., Myhre, A., 2004. Direct human influence of irrigation on atmospheric water vapour and climate. *Clim. Dyn.* 22 (6–7), 597–603. <https://doi.org/10.1007/s00382-004-0402-4>.
- Brocca, L., Ciabatta, L., Massari, C., Moramarco, T., Hahn, S., Hasenauer, S., ... Levizzani, V., 2014. Soil as a natural rain gauge: estimating global rainfall from satellite soil moisture data. *J. Geophys. Res. Atmos.* 119 (9), 5128–5141. <https://doi.org/10.1002/2014JD021489>.
- Campra, P., Garcia, M., Canton, Y., Palacios-Orueta, A., 2008. Surface temperature cooling trends and negative radiative forcing due to land use change toward greenhouse farming in southeastern Spain. *J. Geophys. Res. Atmos.* 113 (D18).
- Chen, Y., Niu, J., Kang, S., Zhang, X., 2018. Effects of irrigation on water and energy balances in the Heihe River basin using VIC model under different irrigation scenarios. *Sci. Total Environ.* 645, 1183–1193.
- Cheng, W., Moore, J.C., Cao, L., Ji, D., Zhao, L., 2017. Simulated climate effects of desert irrigation geoengineering. *Sci. Rep.* 7, 46443. <https://doi.org/10.1038/srep46443>.
- Cho, E., Su, C.H., Ryu, D., Kim, H., Choi, M., 2017. Does AMSR2 produce better soil moisture retrievals than AMSR-E over Australia? *Remote Sens. Environ.* 188, 95–1005.
- Ciabatta, L., Massari, C., Brocca, L., Gruber, A., Reimer, C., Hahn, S., ... Wagner, W., 2018. *SM2RAIN-CCI*: a new global long-term rainfall data set derived from ESA CCI soil moisture. *Earth Syst. Sci. Data* 10 (1), 267.
- Dee, D.P., Uppala, S.M., Simmons, A.J., Berrißord, P., Poli, P., Kobayashi, S., ... Vitart, F., 2011. The ERA-Interim reanalysis: configuration and performance of the data assimilation system. *Q. J. R. Meteorol. Soc.* 137 (656), 553–597. <https://doi.org/10.1002/qj.828>.
- Douglas, E.M., Beltrán-Przekurat, A., Niyogi, D., Pielke, R.A., Vörösmarty, C.J., 2009. The impact of agricultural intensification and irrigation on land-atmosphere interactions and Indian monsoon precipitation – A mesoscale modeling perspective. *Glob. Planet. Chang.* 67 (1), 117–128. <https://doi.org/10.1016/j.gloplacha.2008.12.007>.
- Droogers, P., 2002. *Global Irrigated Area Mapping: Overview and Recommendations: IWMI*.
- Entekhabi, D., Njoku, E.G., O'Neill, P.E., Kellogg, K.H., Crow, W.T., Edelstein, W.N., ... Kimball, J., 2010. The soil moisture active passive (SMAP) mission. *Proceedings of the IEEE* 98 (5), 704–716.
- Evans, R.G., Sadler, E.J., 2008. Methods and technologies to improve efficiency of water use. *Water Resour. Res.* 44 (7). <https://doi.org/10.1029/2007WR006200>.
- Ferguson, C. R., & Wood, E. F. (2011). Observed land-atmosphere coupling from satellite remote sensing and reanalysis. *Journal of Hydrometeorology*, 12(6), 1221–1254.
- Garand, L., 2003. Toward an integrated land-ocean surface skin temperature analysis from the variational assimilation of infrared radiances. *J. Appl. Meteorol.* 42 (5), 570–583. [https://doi.org/10.1175/1520-0450\(2003\)042<0570:TIAOL>2.0.CO;2](https://doi.org/10.1175/1520-0450(2003)042<0570:TIAOL>2.0.CO;2).
- Gordon, L.J., Steffen, W., Jönsson, B.F., Folke, C., Falkenmark, M., Johannessen, A., 2005. Human modification of global water vapor flows from the land surface. *Proc. Natl. Acad. Sci.* 102 (21), 7612–7617. <https://doi.org/10.1073/pnas.0500208102>.
- Gruber, A., Su, C. H., Zwieback, S., Crow, W., Dorigo, W., & Wagner, W. (2016). Recent advances in (soil moisture) triple collocation analysis. *International Journal of Applied Earth Observation and Geoinformation*, 45 (doi:<https://doi.org/10.1016/j.jag.2015.09.002>), 200–211. doi:<https://doi.org/10.1016/j.jag.2015.09.002>
- Gruber, A., Dorigo, W.A., Crow, W., Wagner, W., 2017. Triple collocation-based merging of satellite soil moisture retrievals. *IEEE Trans. Geosci. Remote Sens.* 55 (12), 6780–6792. <https://doi.org/10.1109/TGRS.2017.2734070>.
- Hao, Z., Singh Vijay, P., & Xia, Y. (2018). Seasonal drought prediction: advances, challenges, and future prospects. *Rev. Geophys.*, 0(0). doi:<https://doi.org/10.1002/2016RG000549>.
- Hijmans, R.J., Cameron, S.E., Parra, J.L., Jones, P.G., Jarvis, A., 2005. Very high resolution interpolated climate surfaces for global land areas. *Int. J. Climatol.* 25 (15), 1965–1978.

- Kerr, Y.H., Waldteufel, P., Wigneron, J.P., Martinuzzi, J.A.M.J., Font, J., Berger, M., 2001. Soil moisture retrieval from space: The Soil Moisture and Ocean Salinity (SMOS) mission. *IEEE Trans. Geosci. Remote Sens.* 39 (8), 1729–1735.
- Khan, Muhammad Sarfraz, et al., 2018. Stand-alone uncertainty characterization of GLEAM, GLDAS and MOD16 evapotranspiration products using an extended triple collocation approach. *Agric. For. Meteorol.* 252, 256–268.
- Kim, H., Lakshmi, V., 2018. Use of Cyclone Global Navigation Satellite System (CYGNSS) observations for estimation of soil moisture. *Geophys. Res. Lett.* 45 (16), 8272–8282.
- Kim, H., Lakshmi, V., 2019. Global Dynamics of Stored Precipitation Water in the Topsoil Layer from Satellite and Reanalysis Data. *Water Resour. Res.*
- Kim, H., Parinussa, R., Konings, A. G., Wagner, W., Cosh, M. H., Lakshmi, V., ... Choi, M. (2018). Global-scale assessment and combination of SMAP with ASCAT (active) and AMSR2 (passive) soil moisture products. *Remote Sens. Environ.*, 204, 260–275. doi:<https://doi.org/10.1016/j.rse.2017.10.026>.
- Kumar, S.V., Peters-Lidard, C.D., Santanello, J.A., Reichle, R.H., Draper, C.S., Koster, R.D., ... Jasinski, M.F., 2015. Evaluating the utility of satellite soil moisture retrievals over irrigated areas and the ability of land data assimilation methods to correct for unmodeled processes. *Hydrol. Earth Syst. Sci.* 19 (11), 4463–4478. <https://doi.org/10.5194/hess-19-4463-2015>.
- Lawston, P.M., Santanello, J.A., Zaitchik, B.F., Rodell, M., 2015. Impact of irrigation methods on land surface model Spinup and initialization of WRF forecasts. *J. Hydrometeorol.* 16 (3), 1135–1154. <https://doi.org/10.1175/JHM-D-14-0203.1>.
- Lawston, P.M., Santanello Jr., J.A., Franz, T.E., Rodell, M., 2017. Assessment of irrigation physics in a land surface modeling framework using non-traditional and human-practice datasets. *Hydrol. Earth Syst. Sci.* 21 (6), 2953–2966.
- Lawston, P. M., Santanello Joseph, A., & Kumar Sujay, V. (2018). Irrigation signals detected from SMAP soil moisture retrievals. *Geophysical Research Letters*, 44 (23), 11, 860–811, 867. doi:<https://doi.org/10.1002/2017GL075733>
- Liu, Y.Y., Dorigo, W.A., Parinussa, R.M., de Jeu, R.A.M., Wagner, W., McCabe, M.F., ... van Dijk, A.J.M., 2012. Trend-preserving blending of passive and active microwave soil moisture retrievals. *Remote Sens. Environ.* 123, 280–297. <https://doi.org/10.1016/j.rse.2012.03.014>.
- Liu, X., Yu, L., Li, W., Peng, D., Zhong, L., Li, L., ... Gong, P. (2018). Comparison of country-level cropland areas between ESA-CCI land cover maps and FAOSTAT data. *International Journal of Remote Sensing*, 1–15.
- Lobell, D.B., Bonfill, C., 2008. The effect of irrigation on regional temperatures: a spatial and temporal analysis of trends in California, 1934–2002. *J. Clim.* 21 (10), 2063–2071. <https://doi.org/10.1175/2007JCLI1755.1>.
- Loveland, T. R., Reed, B. C., Brown, J. F., Ohlen, D. O., Zhu, Z., Yang, L., & Merchant, J. W. (2000). Development of a global land cover characteristics database and IGBP DISCover from 1 km AVHRR data. *International Journal of Remote Sensing*, 21 (6–7), 1303–1330. doi:<https://doi.org/10.1080/014311600210191>.
- McDonald, R.I., Girvetz, E.H., 2013. Two challenges for U.S. irrigation due to climate change: increasing irrigated area in wet states and increasing irrigation rates in dry states. *PLOS ONE* 8 (6), e65589. <https://doi.org/10.1371/journal.pone.0065589>.
- Meier, J., Zabel, F., Mauser, W., 2018. A global approach to estimate irrigated areas – a comparison between different data and statistics. *Hydrol. Earth Syst. Sci.* 22 (2), 1119–1133. <https://doi.org/10.5194/hess-22-1119-2018>.
- Molden, D., 2007. *Water for Food, Water for Life: A Comprehensive Assessment of Water Management in Agriculture*: Earthscan.
- Oki, T., Kanae, S., 2006. Global hydrological cycles and world water resources. *Science* 313 (5790), 1068–1072. <https://doi.org/10.1126/science.112845>.
- Oleson, K.W., Bonan, G.B., Schaaf, C., Gao, F., Jin, Y., Strahler, A., 2003. Assessment of global climate model land surface albedo using MODIS data. *Geophys. Res. Lett.* 30 (8). <https://doi.org/10.1029/2002GL016749>.
- Ozdogan, M., Gutman, G., 2008. A new methodology to map irrigated areas using multi-temporal MODIS and ancillary data: an application example in the continental US. *Remote Sens. Environ.* 112 (9), 3520–3537. <https://doi.org/10.1016/j.rse.2008.04.010>.
- Ozdogan, M., Woodcock, C.E., 2006. Resolution dependent errors in remote sensing of cultivated areas. *Remote Sens. Environ.* 103 (2), 203–217. <https://doi.org/10.1016/j.rse.2006.04.004>.
- Ozdogan, M., Yang, Y., Allez, G., Cervantes, C., 2010. Remote sensing of irrigated agriculture: opportunities and challenges. *Remote Sens.* 2 (9), 2274–2304. <https://doi.org/10.3390/rs2092274>.
- Pielke, Pitman A., Niyogi, D., Mahmood, R., McAlpine, C., Hossain, F., ... de Noblet, N. (2011). Land use/land cover changes and climate: modeling analysis and observational evidence. *Wiley Interdiscip. Rev. Clim. Chang.*, 2(6), 828–850. doi:<https://doi.org/10.1002/wcc.144>.
- Pryor, S.C., Sullivan, R.C., Wright, T., 2016. Quantifying the roles of changing albedo, emissivity, and energy partitioning in the impact of irrigation on atmospheric heat content. *J. Appl. Meteorol. Climatol.* 55 (8), 1699–1706. <https://doi.org/10.1175/JAMC-D-15-0291.1>.
- Puma, M.J., Cook, B.I., 2010. Effects of irrigation on global climate during the 20th century. *J. Geophys. Res. Atmos.* 115 (D16). <https://doi.org/10.1029/2010JD014122>.
- Qian, Y., Huang, M., Yang, B., Berg, L.K., 2013. A modeling study of irrigation effects on surface fluxes and land-air-cloud interactions in the southern Great Plains. *J. Hydrometeorol.* 14 (3), 700–721. <https://doi.org/10.1175/JHM-D-12-0134.1>.
- Qiu, J., Gao, Q., Wang, S., Su, Z., 2016. Comparison of temporal trends from multiple soil moisture data sets and precipitation: the implication of irrigation on regional soil moisture trend. *Int. J. Appl. Earth Obs. Geoinf.* 48, 17–27. <https://doi.org/10.1016/j.jag.2015.11.012>.
- Riediger, J., Breckling, B., Nuske, R.S., Schröder, W., 2014. Will climate change increase irrigation requirements in agriculture of Central Europe? A simulation study for Northern Germany. *Environ. Sci. Eur.* 26 (1), 18. <https://doi.org/10.1186/s12302-014-0018-1>.
- Rosenzweig, C., Strzepek, K.M., Major, D.C., Iglesias, A., Yates, D.N., McCluskey, A., Hillel, D., 2004. Water resources for agriculture in a changing climate: international case studies. *Glob. Environ. Chang.* 14 (4), 345–360. <https://doi.org/10.1016/j.gloenvcha.2004.09.003>.
- Ryan, E.M., Ogle, K., Peltier, D., Walker Anthony, P., De Kauwe Martin, G., Medlyn Belinda, E., ... Pendall, E., 2017. Gross primary production responses to warming, elevated CO₂, and irrigation: quantifying the drivers of ecosystem physiology in a semiarid grassland. *Glob. Chang. Biol.* 23 (8), 3092–3106. <https://doi.org/10.1111/gcb.13602>.
- Sacks, W.J., Cook, B.I., Buenning, N., Lewis, S., Helkowski, J.H., 2009. Effects of global irrigation on the near-surface climate. *Clim. Dyn.* 33 (2–3), 159–175. <https://doi.org/10.1007/s00382-008-0445-z>.
- Salmon, J.M., Friedl, M.A., Frolking, S., Wisser, D., Douglas, E.M., 2015. Global rain-fed, irrigated, and paddy croplands: A new high resolution map derived from remote sensing, crop inventories and climate data. *Int. J. Appl. Earth Obs. Geoinf.* 38, 321–334. <https://doi.org/10.1016/j.jag.2015.01.014>.
- Schultz, B., Thatte, C.D., Labhsetwar, V.K., 2005. Irrigation and drainage. Main contributors to global food production. *Irrig. Drain.* 54 (3), 263–278. <https://doi.org/10.1002/ird.170>.
- Shi, W., Tao, F., Liu, J., 2014. Regional temperature change over the Huang-Huai-Hai Plain of China: the roles of irrigation versus urbanization. *Int. J. Climatol.* 34 (4), 1181–1195. <https://doi.org/10.1002/joc.3755>.
- Siebert, S., Döll, P., Hoogeveen, J., Faures, J.M., Frenken, K., Feick, S., 2005. Development and validation of the global map of irrigation areas. *Hydrol. Earth Syst. Sci. Discuss.* 2 (4), 1299–1327.
- Siebert, S., Henrich, V., Frenken, K., & Burke, J. (2013). Update of the Global Map of Irrigation Areas to version 5. Project report, 178.
- Singh, D., Gupta, P., Pradhan, R., Dubey, A., Singh, R., 2017. Discerning shifting irrigation practices from passive microwave radiometry over Punjab and Haryana. *J. Water Clim. Change* 8 (2), 303–319.
- Taylor, C.M., Jeu, R.A.M.d., Guichard, F., Harris, P.P., Dorigo, W.A., 2012. Afternoon rain more likely over drier soils. *Nature* 489 (7416), 423–426. <https://doi.org/10.1038/nature11377>.
- Thenkabail, P.S., Biradar, C.M., Noojipady, P., Dheeravath, V., Li, Y., Velpuri, M., ... Dutta, R., 2009. Global irrigated area map (GIAM), derived from remote sensing, for the end of the last millennium. *Int. J. Remote Sens.* 30 (14), 3679–3733. <https://doi.org/10.1080/01431160802698919>.
- Trigo, I.F., Viterbo, P., 2003. Clear-sky window channel radiances: a comparison between observations and the ECMWF model. *J. Appl. Meteorol.* 42 (10), 1463–1479. [https://doi.org/10.1175/1520-0450\(2003\)042<1463:CWRAC>2.0.CO;2](https://doi.org/10.1175/1520-0450(2003)042<1463:CWRAC>2.0.CO;2).
- Trigo, I. F., Boussetta, S., Viterbo, P., Balsamo, G., Beljaars, A., & Sandu, I. (2015). Comparison of model land skin temperature with remotely sensed estimates and assessment of surface-atmosphere coupling. *Journal of Geophysical Research: Atmospheres*, 120 (23), 12, 096–012, 111. doi:<https://doi.org/10.1002/2015JD023812>
- Tsvetinskaya, E.A., Schaaf, C.B., Gao, F., Strahler, A.H., Dickinson, R.E., Zeng, X., Lucht, W., 2002. Relating MODIS-derived surface albedo to soils and rock types over Northern Africa and the Arabian peninsula. *Geophys. Res. Lett.* 29 (9), 67–1–67–4. <https://doi.org/10.1029/2001GL014096>.
- Tuinenburg, O. A., & Vries, J. P. R. (2017). Irrigation patterns resemble ERA-interim reanalysis soil moisture additions. *Geophysical Research Letters*, 44 (20), 10, 341–310, 348. doi:<https://doi.org/10.1020/2017GL074884>
- Umair, M., Kim, D., Ray, R.L., Choi, M., 2018. Estimating land surface variables and sensitivity analysis for CLM and VIC simulations using remote sensing products. *Sci. Total Environ.* 633, 470–483.
- Vahmani, P., Hogue, T.S., 2014. Incorporating an urban irrigation module into the Noah land surface model coupled with an urban canopy model. *J. Hydrometeorol.* 15 (4), 1440–1456.
- Vörösmarty, C.J., Sahagian, D., 2000. Anthropogenic disturbance of the terrestrial water cycle. *BioScience* 50 (9), 753–765. [https://doi.org/10.1641/0006-3568\(2000\)050\[0753:ADOTTW\]2.0.CO;2](https://doi.org/10.1641/0006-3568(2000)050[0753:ADOTTW]2.0.CO;2).
- Vörösmarty, C.J., Green, P., Salisbury, J., Lammers, R.B., 2000. Global water resources: vulnerability from climate change and population growth. *Science* 289 (5477), 284–288. <https://doi.org/10.1126/science.289.5477.284>.
- Wagner, W., Hahn, S., Kidd, R., Melzer, T., Bartalis, Z., Hasenauer, S., ... Komma, J., 2013. The ASCAT soil moisture product: A review of its specifications, validation results, and emerging applications. *Meteorol. Z.* 22 (1), 5–33.
- Wang, A., Barlage, M., Zeng, X., Draper Clara, S., 2014. Comparison of land skin temperature from a land model, remote sensing, and in situ measurement. *J. Geophys. Res. Atmos.* 119 (6), 3093–3106. <https://doi.org/10.1002/2013JD021026>.
- Wei, H., Xia, Y., Mitchell, K.E., Ek, M.B., 2013a. Improvement of the Noah land surface model for warm season processes: evaluation of water and energy flux simulation. *Hydrolog. Process.* 27 (2), 297–303.
- Wei, J., Dirmyer, P. A., Wisser, D., Bosilovich, M. G., & Mocko, D. M. (2013b). Where does the irrigation water go? An estimate of the contribution of irrigation to precipitation using MERRA. *J. Hydrometeorol.*, 14(1), 275–289.
- Wisser, D., Frolking, S., Douglas Ellen, M., Fekete Balazs, M., Vörösmarty Charles, J., Schumann Andreas, H., 2008. Global irrigation water demand: variability and uncertainties arising from agricultural and climate data sets. *Geophys. Res. Lett.* 35 (24). <https://doi.org/10.1029/2008GL035296>.
- Wisser, D., Fekete, B.M., Vörösmarty, C.J., Schumann, A.H., 2010. Reconstructing 20th century global hydrography: a contribution to the Global Terrestrial Network-Hydrology (GTN-H). *Hydrol. Earth Syst. Sci.* 14 (1), 1–24. <https://doi.org/10.5194/hess-14-1-2010>.
- Wood, E.F., Roundy, J.K., Troy, T.J., Van Beek, L., Bierkens, M.F., Blyth, E., ... Famiglietti, J., 2011. Hyperresolution global land surface modeling: meeting a grand challenge for monitoring Earth's terrestrial water. *Water Resour. Res.* 47 (5).
- Zabel, F., Putzenlechner, B., Mauser, W., 2014. Global agricultural land resources—a high resolution suitability evaluation and its perspectives until 2100 under climate change conditions. *PLoS One* 9 (9), e107522.

- Zaussinger, F., Dorigo, W., Gruber, A., Tarpanelli, A., Filippucci, P., Brocca, L., 2019. Estimating irrigation water use over the contiguous United States by combining satellite and reanalysis soil moisture data. *Hydrol. Earth Syst. Sci.* 23 (2), 897–923.
- Zeng, Y., Xie, Z., Liu, S., Xie, J., Jia, B., Qin, P., Gao, J., 2018. Global land surface modeling including lateral groundwater flow. *J. Adv. Model. Earth Syst.* 10 (8), 1882–1900.
- Zhang, T., Lin, X., 2016. Assessing future drought impacts on yields based on historical irrigation reaction to drought for four major crops in Kansas. *Sci. Total Environ.* 550, 851–860.
- Zhang, X., Qiu, J., Leng, G., Yang, Y., Gao, Q., Fan, Y., Luo, J., 2018. The potential utility of satellite soil moisture retrievals for detecting irrigation patterns in China. *Water* 10 (11), 1505.
- Zhao, G., Webber, H., Hoffmann, H., Wolf, J., Siebert, S., Ewert, F., 2015. The implication of irrigation in climate change impact assessment: a European-wide study. *Glob. Chang. Biol.* 21 (11), 4031–4048. <https://doi.org/10.1111/gcb.13008>.
- Zheng, W., Wei, H., Wang, Z., Zeng, X., Meng, J., Ek, M., ... Derber, J., 2012. Improvement of daytime land surface skin temperature over arid regions in the NCEP GFS model and its impact on satellite data assimilation. *J. Geophys. Res. Atmos.* 117 (D6). <https://doi.org/10.1029/2011JD015901>.
- Zhou, L., Dickinson, R.E., Tian, Y., Fang, J., Li, Q., Kaufmann, R.K., ... Myneni, R.B., 2004. Evidence for a significant urbanization effect on climate in China. *Proc. Natl. Acad. Sci.* 101 (26), 9540–9544. <https://doi.org/10.1073/pnas.0400357101>.
- Zhuo, L., Han, D., 2017. Hydrological Evaluation of Satellite Soil Moisture Data in Two Basins of Different Climate and Vegetation Density Conditions (Advances in Meteorology).
- Zohaib, M., Kim, H., Choi, M., 2017. Evaluating the patterns of spatiotemporal trends of root zone soil moisture in major climate regions in East Asia. *J. Geophys. Res. Atmos.* 122 (15), 7705–7722. <https://doi.org/10.1002/2016JD026379>.